JOURNAL OF MATERIALS SCIENCE 28 (1993) 999 – 1006

Application of phase shifting interferential microscopy to pitting corrosion studies of ion-implanted stainless steel

R. ESCALONA, R.DEVILLERS, G. TRIBILLON
Laboratoire d'Optique P. M. Duffieux, URA CNRS 214, Université de Franche-Comté, 25030 Besançon Cédex, France

J. CALATRONI
Dep. Fisica, Universidad Simon Bolivar, A.P. 89000, Caracas 080-A, Venezuela

P.FIEVET, Y. ROQUES, F. DABOSI
Laboratoire de Métallurgie Physique, URA CNRS 445, Ecole Nationale Supérieure de Chimie, 118, route de Narbonne 31077 Toulouse Cédex, France.

Phase-shifting interferometry microscopy is applied to the analysis of corrosion pitting of a 304 stainless steel (with and without molybdenum-ion implantation) in NaCl solution. Owing to the dimensions of the pits two kinds of pit can be defined. The statistical analysis of the specimen-inspected field shows that small pits of area $< 50\ \mu m^2$ are by far the most frequent. The different sizes of the pits can be related to the different stages of pit formation, pre-pitting and growth.

1. Introduction

Localized corrosion of metals and alloys is a very important subject largely due to economic reasons. This is particularly the case for stainless steels in chloride media. In a bibliographical review [1], Sklarska-Smialowska shows that rather complex phenomena are involved and that very few experimental techniques allow the study of the initial phases of corrosion. Nowadays, most of the authors agree that pitting corrosion has a stochastic character [2], but the experimental procedures used are essentially electrochemical techniques.

Another experimental approach to the study of pitting corrosion is to use optical techniques. Recently [3], a statistical analysis of the evolution of the corrosion process was done by digital processing of the image of the sample surface. This is a useful technique when the corrosion involves small quantities of matter, so that electrochemical techniques cannot be applied. Thus the spatial distribution of the pits, and the surface dimensions of individual pits can be obtained, but there is no information on pit depth.

Here, we present the application of a recent procedure of optical microscopy to the analysis of localized corrosion. The technique, which is called "phase-shifting interferential microscopy" (PSIM) allows one to obtain the profile $z(x;y)$ of the surface under corrosion with a high precision: depth resolution of $\delta z \approx 1$ nm and lateral resolution $\delta x \approx 300$ nm are currently obtained. The same technique was recently used by Kragt *et al.* [4] to observe the evolution of a single corrosion pit in an iron electrode. However, no measurements were done concerning the statistical distribution in depth and area of the pits in the inspected region. The aim of this work was to apply PSIM to the measurement of physical dimensions of corrosion pits, i.e. the actual profile of the surface of the specimen $z(x;y)$ where a field of pits has grown, the area of each pit in the plane of the surface and the volume of each pit in the inspected field. The application of PSIM to automatic measurements of the surface and of the volume of each small pit in a corrosion field is presented here.

We have applied PSIM to the analysis of 304 stainless steel alloys implanted and unimplanted with molybdenum in NaCl solution. Basically, the experimental system consists of a modified optical interference microscope in which the image of the sample surface is numerically processed by a microcomputer. By means of software which has been specifically developed, the number of pits, their area and volume are automatically calculated for each inspected region. The statistical distribution of the area of the pits is presented, as well as the volume-to-surface relation. Those results show that for small pits of area smaller than 16 μm^2, the depth grows with the surface of the hole. On the other hand, for pits of a bigger area, the growth in surface becomes more important than in depth. Even though the experimental results presented here are the first of their kind, they show that the molybdenum prevents the growth of the pits. The procedure of PSIM is briefly described and the experimental details are presented, and the results obtained are discussed.

0022–2461

2. Phase-shifting interferential microscopy (PSIM)

In order to present a qualitative description of PSIM let us first refer to the classical procedure for interference microscopy. As is well known, the interference technique has been widely used in metallography where a quantitative knowledge of depth features of the specimen surface is needed.

The method involves the use of a microscope with an interferential objective. Fig. 1 shows a diagram of the light rays in a Mireau interferential objective. The light coming from the source is divided into two beams by a beam splitter. One of the beams is reflected by the specimen and the other is reflected by the reference mirror. After reflection, both beams are superimposed at the beam splitter and return to the eyepiece or the detector array. The superposition of the two beams which have travelled along different paths gives rise to an interference pattern. As a result, the enlarged image of the specimen which is formed by the objective appears crossed by a series of bright and dark fringes. Each fringe behaves as a level curve of the surface. The depth difference between two adjacent fringes is half the wavelength ($\lambda/2$) of the light source. The interference image (i.e. the image of the specimen with the interference pattern) can be detected by a pixel array and then sent to a microcomputer in order to obtain information about the profile from the level curve. However, this procedure has two main drawbacks.

1. The surface profile is ambiguous, because from the interference pattern it is not possible to distinguish the hills from the valleys in the sample surface. All that can be known is the absolute value of the height difference between two consecutive fringes. In order to have the real surface profile, complementary information must be added.

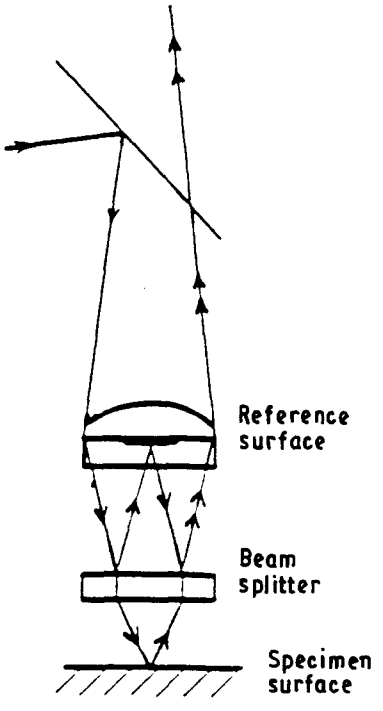

Figure 1 Objective, × 40, with modified Mireau interferometer.

2. The depth resolution is limited to $\lambda/4$ (≈ 150 nm), because quantitative information from the fringe pattern can only be obtained reliably from the maxima and minima of the interference fringes. Any interpolation between the fringes is long, difficult, and not very accurate.

Both previous disadvantages are overcome by phase-shifting interferometry (PSI): the surface profile is obtained without any kind of ambiguity, with a depth resolution as high as $\delta z \approx 1$ nm.

The basic idea of PSI is to record several interference images instead of only one as before. Indeed, four images are recorded under four different conditions. From one image to the next, the path difference between the interference beams is changed in $\lambda/4$ steps. Each interference image is recorded by means of a two-dimensional pixel array (CCD camera) and stored in a memory card. This means that for each point of the image (which corresponds to a particular point in the surface) four different values of the local light intensity are measured. Then, the surface profile can be calculated as described by Tiziani [5] and Pieralli and Tribillon [6]

$$z(x;y) = \lambda/4 \text{ arc tg } \{[I_4(x;y) - I_2(x;y)]/[I_1(x;y) - I_3(x;y)]\} \quad (1)$$

where $I_1(x;y)$, $I_2(x;y)$, $I_3(x;y)$, $I_4(x;y)$ are the local values of the light intensity for the four additional path differences of 0, $\lambda/4$, $\lambda/2$ and 3 $\lambda/4$, respectively, $z(x;y)$ is the surface profile, λ is the wavelength of the light source.

Equation 1 shows that the surface profile is calculated for each point in the surface in an independent way, instead of a relation between the height of each point and the height of its neighbour. This is the most important fact of the method, and the reason for the high vertical resolution. When the path difference is changed in steps of $\lambda/4$, the light intensity in each point of the image varies as a cosinus function, and then, the constant part of the path difference, $z(x;y)$, can be obtained. From Equation 1 it can be seen that the vertical resolution, dz, is related to the intensity resolution (the reciprocal of the number of grey levels in which the light intensity is quantified) rather than to the lateral resolution.

In fact, the surface profile is not completely known from Equation 1 because the arc tg can be found only within some multiple of 2^8. However, knowing that $z(x;y)$ is a continuous function, $\lambda/2$ discontinuities are easily resolved by comparing adjacent points and adding or subtracting $\lambda/2$ until the height difference between adjacent pixels is less than $\lambda/2$. This correction to the surface profile is automatically done by the image processing software.

The most common way to change the path difference between the two interference beams is to mount the reference mirror in a piezoelectric transducer (PZT) and to change the voltage of the PZC. Thus the basic experimental set-up is very similar to that of classical interference microscopy, except for the controlled movement of the reference mirror and the software for the image processing.

Other important advantages of PSI are rapid measurements, good results even with low contrast fringes, and results which are independent of the intensity variations across the surface.

3. Experimental procedure

3.1. Apparatus

The block diagram of the experimental apparatus is shown in Fig. 2. It consists of a metallurgical optical microscope, a CCD camera, an image analogue/digital conversion and memory card; a drive unit for the PZT and a microcomputer. Fig. 3 shows the optical part of the system. As a light detector, a CCD camera of 512 × 512 pixels is used. The area of each pixel is 11 × 11 μm^2. The analogue signal of the CCD camera is digitized in 2^8 grey levels and then sent to a microcomputer.

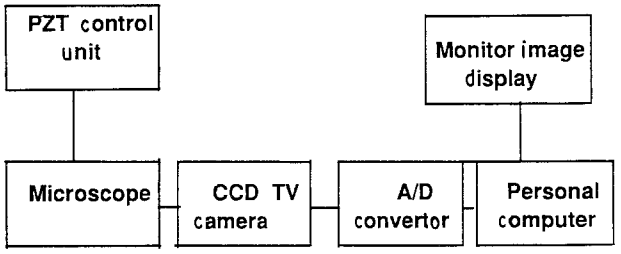

Figure 2 Phase-shifting interferometer microscope block diagram.

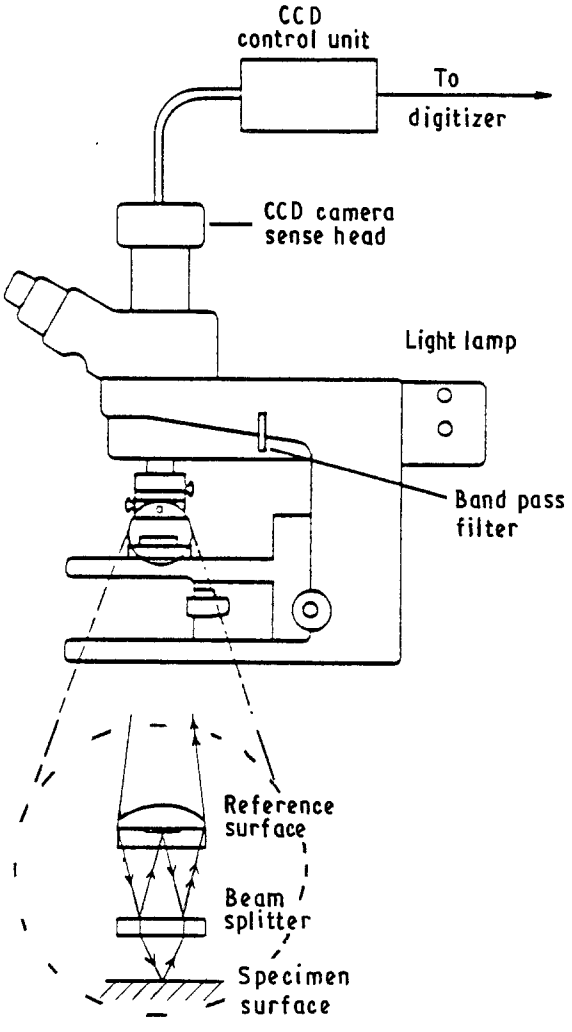

Figure 3 Experimental apparatus.

The theoretical vertical resolution is limited by the number of quantification levels of light intensity. For our 8 bits A/D converter, the theoretical vertical resolution is $dz \approx \lambda/1000$. However, due to the involved noise it is reduced to $\lambda/500$. Lateral resolution is limited by the width of a single pixel in the CCD camera and by the numerical aperture of the microscope objective. For a × 20 objective in our system, $dx \approx 0.5$ μm. The acquisition time for the four images is 0.2 s, and 60 s is the total time for the profile evaluation of an image of 512 × 512 pixels. The performances of our PSIM are summarized in Table I.

The software for image processing plays a very important role in the PSIM. The whole image processing involves several stages: calculus of the height $z(x;y)$ of each point, filtering of the tilt and roughness of the surface, localization of holes, through the analysis of local slopes, recognition and labelling of holes, filling of the contours and calculations of surface and volume of the holes.

The complete phase-shifting interferential microscope was developed at the Laboratoire d'Optique de Besançon, including all the software for microscope driving, PZT control and image processing.

3. 2. Materials and procedure

The material used in this work (samples A, B and C) was AISI Type 304 steel cold rolled with the following composition (mass%): C 0.053, Mn 1.427, Si 0.485, P 0.029, Ni 8.28, Cr 17.38, Mo 0.139, Cu 0.145, Ti 0.002, Al 0.002, N 0.040, B 0.0004. The surface of Samples B and C was modified by Mo^+-ion implantation (2.5 10^{16} at cm^{-2}, 100 keV).

The specimens were in the form of discs of 10 mm diameter mounted in epoxy resin. They were ground with silicon carbide paper up to 4000 grade and cleaned with deionized water.

Solutions were prepared with deionized water and reagent grade NaCl (0.5 $mol\,l^{-1}$), pH being equal to 5.5. Pitting of Sample A was obtained by a 38 h immersion in NaCl solution at open circuit potential. Pitting of Samples B and C was obtained by a 10 min

TABLE I Performances of the PSIM

	Magnification			
	5	10	20	40
Interferometer type	Mireau	Mireau	Mireau	Mireau
Numerical aperture	0.100	0.250	0.400	0.500
Optical resolution (μm)	2.8	1.1	0.69	0.42
Depth resolution (μm)	63	12	4	1, 3
Inspected surface (mm^2): $H \times V$	1.6 × 1.1	0.8 × 0.56	0.4 × 0.28	0.2 × 0.14
Sampling interval (μm):				
H	3.1	1.5	0.79	0.39
V	2.2	1.1	0.55	0.28
Work distance (mm)	4	4	1.9	1.9
Maximum height (μm)	63	12	4	1, 3
Maximum slope (deg.)	3, 8	7, 6	15, 0	27, 7

immersion in NaCl solution followed by a 180 s polarization at 700 and 300 mV/SCE, respectively.

4. Results

Fig. 4a and b show the surface profiles of two different regions of Sample A. The surface profile is reversed before representation so that corrosion pits appear as hills. In Fig. 4a, a large number of small pits is observed while the sample is immersed in the solution at the corrosion potential. The depths of the pits are higher than the passive film layer thickness. However, a macroscopic pit is visible. In Fig. 4b it can be seen that there is a relationship between the density of the pits and the substrate structure.

Fig. 5a and b show the image of the surface for two regions of Sample B. It can be seen that two different kinds of pits are present. A first group of large round pits of diameter $\approx 50\,\mu m$ and depth $\approx 20\,\mu m$ is observed. On the other hand, there is another group of pits smaller in size and depth.

In this work the first kind of large pits was not considered. In fact, they cannot be analysed by our PSIM. The large pits present such high slopes that the hypothesis of continuity for the surface profile is no longer valid. Moreover, large pits can be easily observed and measured by the classical methods of non-interferometric microscopy. Indeed, the study of large pits is not the most important in understanding the mechanism of pitting corrosion, because they correspond to the intermediate state of the phenomenon. On the other hand, small pits are associated with the appearance and evolution of the corrosion process.

Williams *et al.* [7] have considered a model based on a prepitting stage and a stable pitting stage. The large pits of Sample B correspond to the stable stage. They can be analysed by the classical methods of non-interferometric microscopy or by electrochemical methods. In addition, the size of large pits can be related, through Faraday's law, to the current threshold value when electrochemical techniques for pit detection are performed.

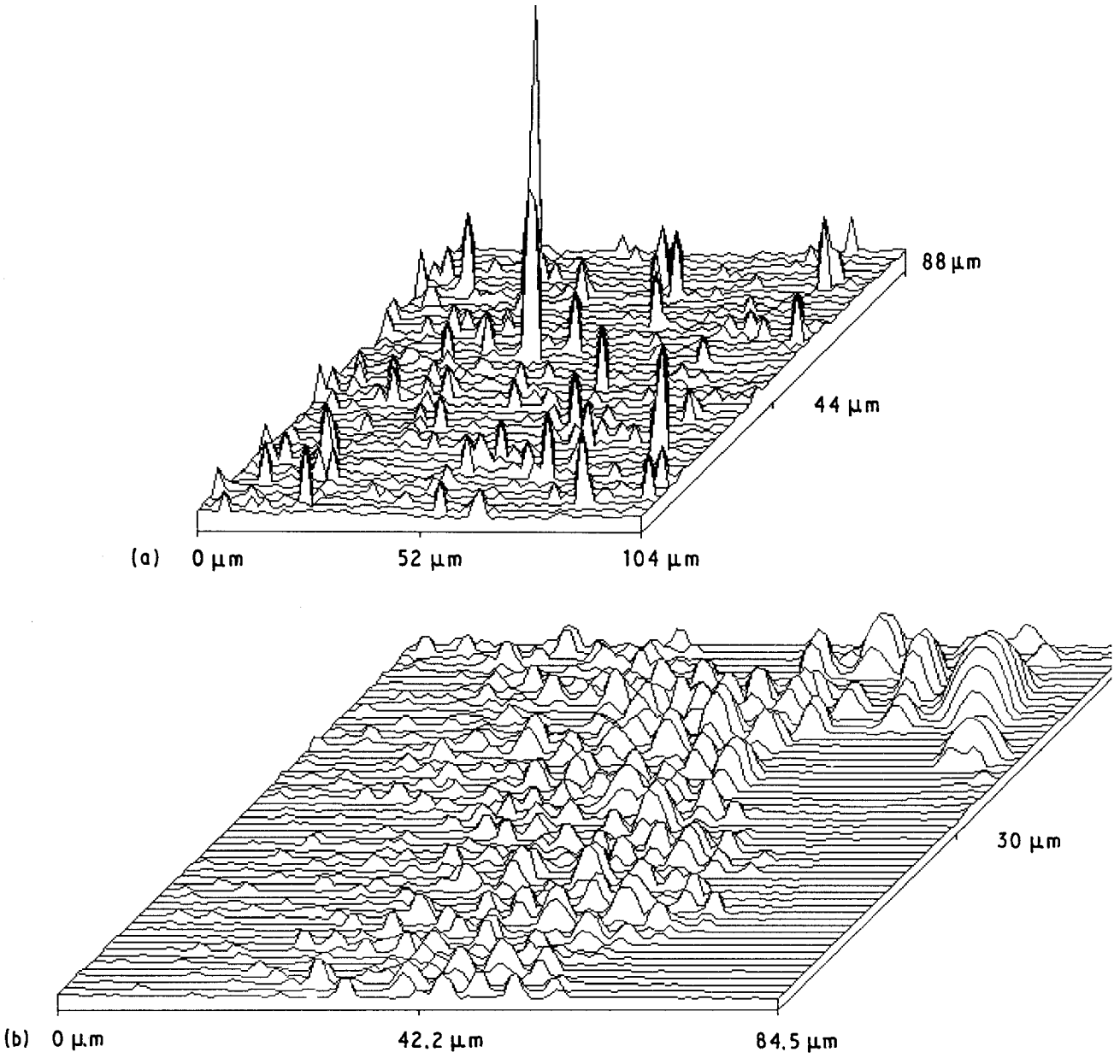

Figure 4 Surface profile of Sample A (un implanted stainless steel after a 38 h immersion in 0.5 mol l^{-1} NaCl solution at the open potential). Two different zones (a) and (b).

Fig. 6a and b show two inverted surface profiles which correspond to different regions in the same Sample B. It can be seen that the three-dimensional display of the surface furnishes a global information about frequency, spatial distribution and relative depths of corrosion pits. The three-dimensional display is also useful to compare the pits with the roughness of the surface. Otherwise, for a more quantitative topographical analysis, the profile of the pit along a selected line (or a row) is sometimes more convenient.

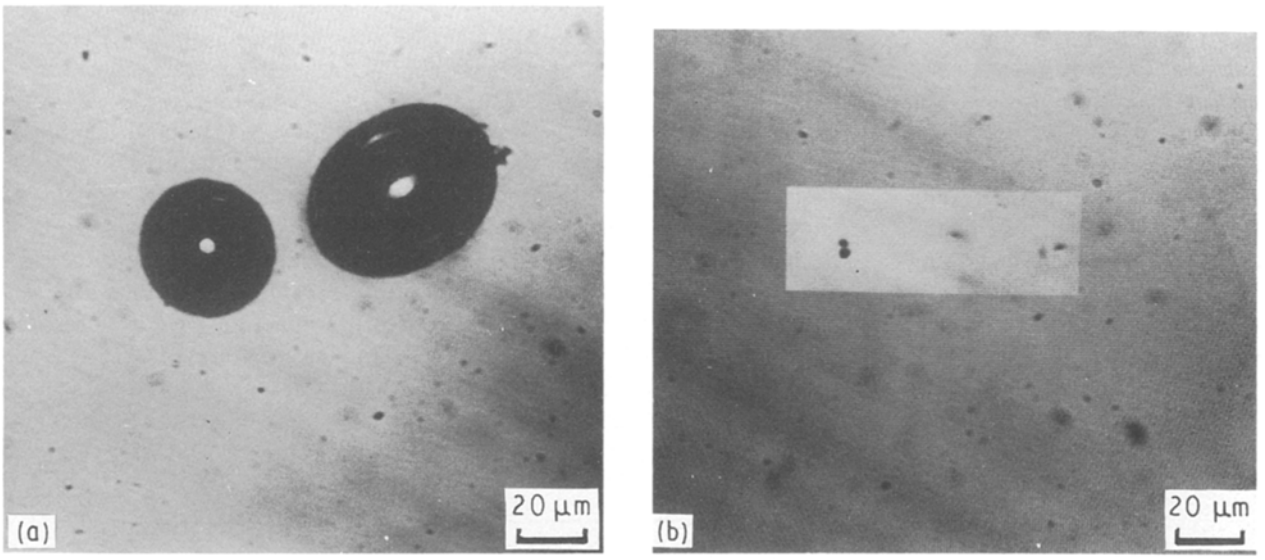

Figure 5 (a, b) Optical micrographs of Sample A (unimplanted stainless steel after a 38 h immersion in 0.5 mol l^{-1} NaCl solution at the open potential).

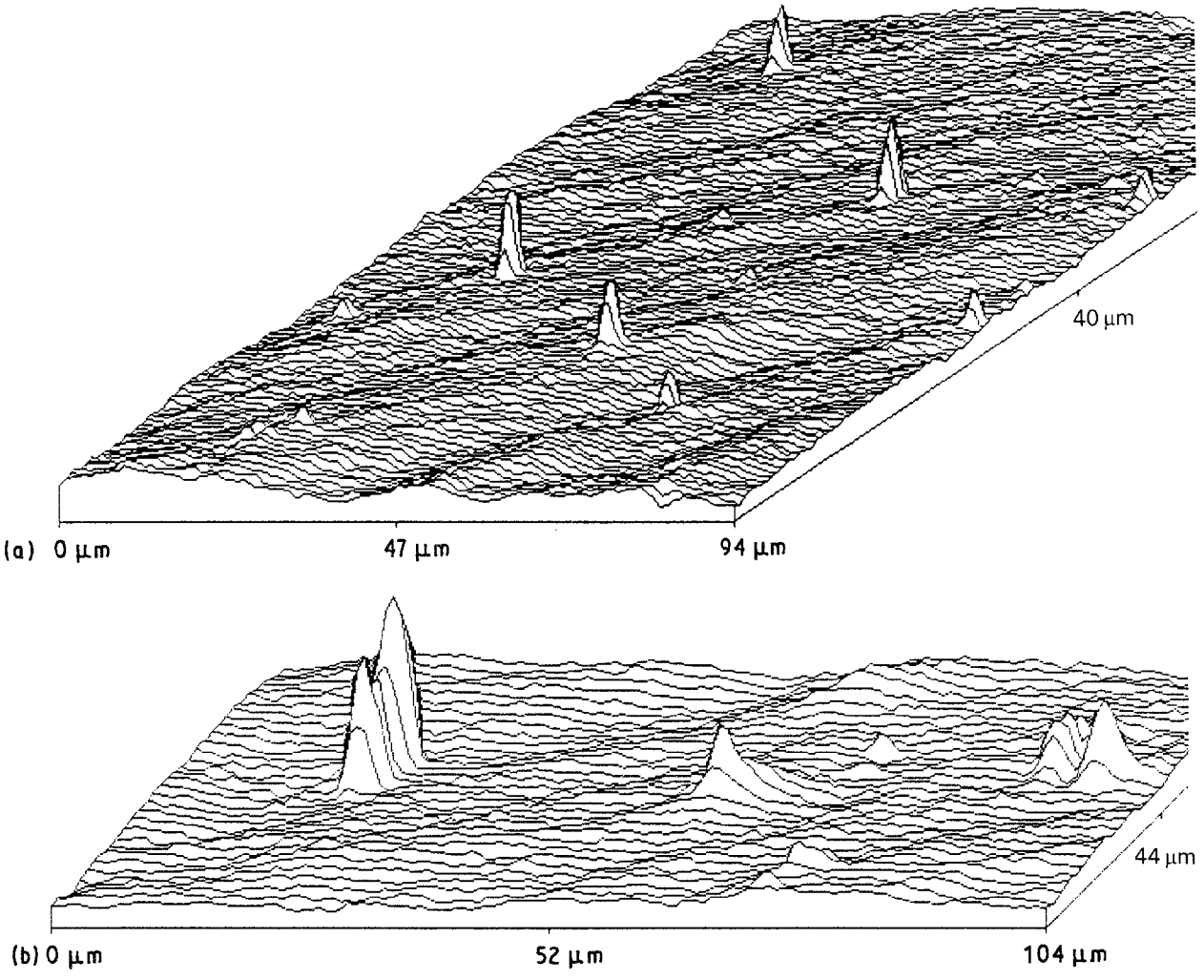

Figure 6 (a, b) Profile of Sample B (molybdenum-ion implanted stainless steel after a 10 min immersion in 0.5 mol l^{-1} NaCl solution at the open potential then 180 s at 700 mV/SCE).

Fig. 7a and b show the profile of the large pit on the left of Fig. 6b. Fig. 7a is the profile along a line and Fig. 7b along a row. It can be seen that the pit has a complex structure which is not evident from the three-dimensional display.

Taking into account the real dimension of pits, it can be seen that they are not as sharp as Fig. 6 suggests at first sight. The pit of Fig. 7a, for example, is 3.75 μm wide and 0.043 μm deep. In fact, the height difference between lateral resolution and vertical resolution makes the method well adapted to the measurements of corrosion pits during their first stage of development.

Table II presents the results of the analysis of the region shown in Fig. 6a. The term "seuil" stands for the threshold level which has been selected to define the top level of the hole. It must be remembered that after processing, the surface profile is represented in a scale of 256 grey levels so that the highest point in the surface is 255 and the bottom is 0. In order to evaluate the surface and the volume of all the pits of a region, we must first define what will be considered as a pit. This is an important choice because it prevents those occasional depressions in the surface being considered as corrosion pits. This selection of the threshold is not unequivocal and it depends on the criterion of each operator. Moreover, different thresholds can be chosen by the same operator from one region to another in the same specimen. In fact, the same situation is present for the volume of a pit. Therefore, it must be considered that the surface and volume measurements are affected by an additional uncertainty due to the lack of uniformity in the threshold definition. The fluctuation in threshold definition is about 10%.

In spite of this, the automatic measurement of surface and volume of all the pits in an inspected field is a useful and quantitative tool to analyse the corrosion degree of a given region of the sample.

Fig. 8 presents a histogram of pit surfaces of Sample C (size < 65 μm^2). Sample C has been polarized under less severe conditions than Sample B; this is the reason why the largest pits have quite different development.

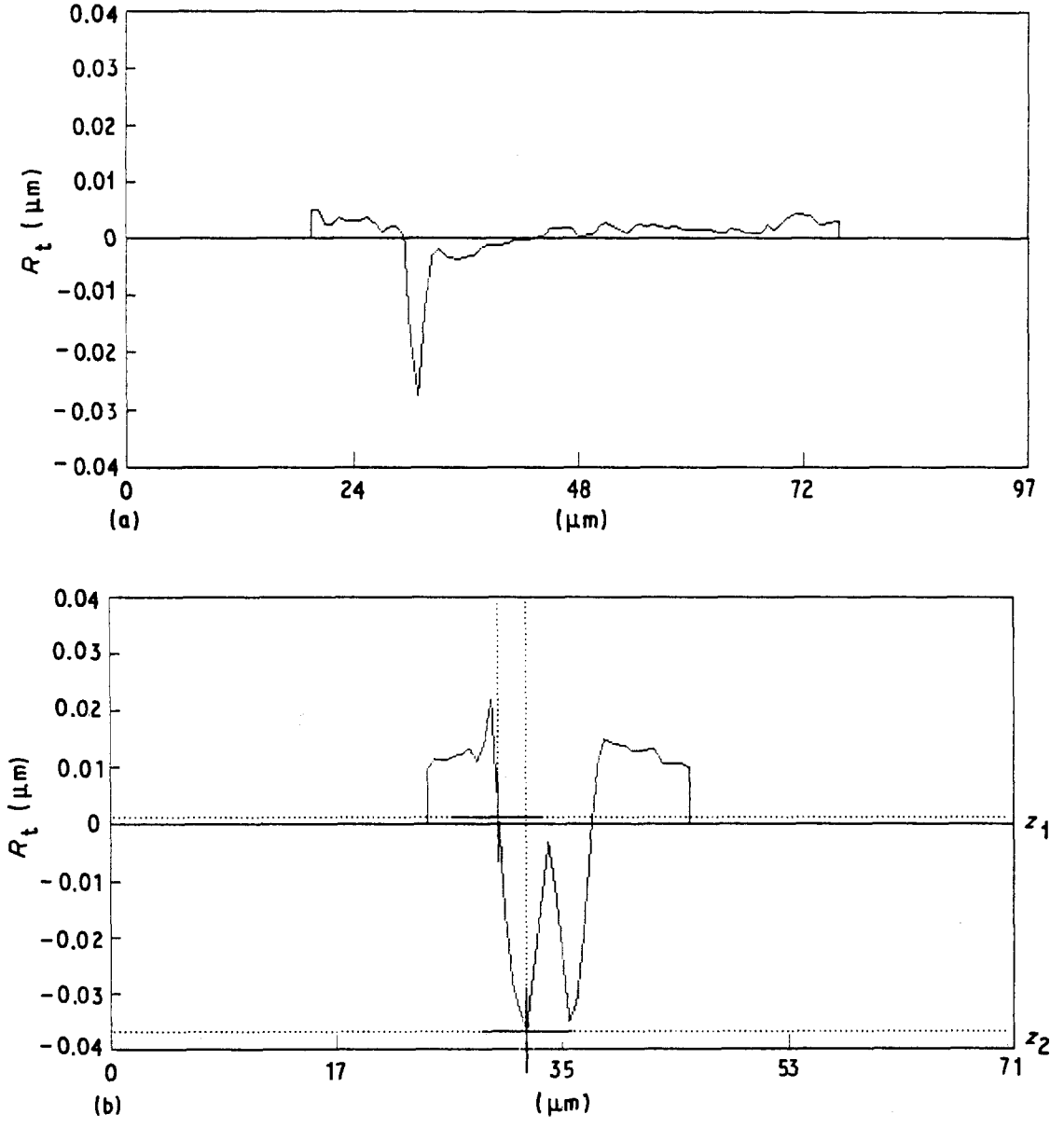

Figure 7 Profile (a) along a line and (b) along a row for Sample B (molybdenum-ion implanted stainless steel after a 10 min immersion in 0.5 mol l^{-1} NaCl solution at the open potential then 180 s at 700 mV/SCE.)

Small pits are very numerous: their volume corresponds to low dissolution current quantities. For unimplanted samples and under potentiostatic conditions, current fluctuations with time are observed. They are related to a prepitting stage with pits of size $< 15\ \mu m^2$. This corresponds to the range investigated by the technique presented in this paper. Some authors consider the current fluctuations to be electrochemical noise and use frequential methods of analysis [8, 9]. Electrochemical techniques do not give individual pieces of information on position, surface and volume dimensions of pits involved. The technique presented here is well adapted to these determinations.

The variation of pit depth presented in Fig. 7b shows that in some cases pits have a complex profile. Under these conditions the volume is a more realistic characteristic of pits than the mean depth. In Fig. 9 a correlation between the apparent surface of the pits and their volume is shown. Suppose a simple model of pit growth with homogeneous attack all over the lateral surface of the pit leads to both a variation of the volume, V, of the pit proportional to R^3, and a variation of the apparent surface, S, proportional to R^2. The relation between V and S is presented in Fig. 9 by the dashed line. It is clear that such a relation is verified for experimental points for low values of V or S. In other cases pits of high surface value are of comparatively low volume. This corresponds to a low depth.

Experimental results show that for the unimplanted Sample A, at the corrosion potential there is no macroscopic hemispherical pit. But this is the case with a polarization in the 300–700 mV/SCE range.

For molybdenum implanted samples in the same 300–700 mV/SCE polarization range, there are very few macroscopic pits and mostly very small pits corresponding to a pre-pitting stage. It can be concluded that the growth of pits is limited by the presence of molybdenum.

The depths of pre-pits in these implanted samples are comparable with the thickness of the implanted zone (50 nm). Indeed, this is also the case for unimplanted samples. So there is no direct relation between the depth of pre-pits and the implanted zone thickness.

The technique presented above allows a quantitative estimation of the pitting corrosion. Future work will be devoted to the investigation of the role of molybdenum in the inhibition of pitting corrosion (effect of molybdenum in the solid phase or the passivating action of molybdate ions in solution).

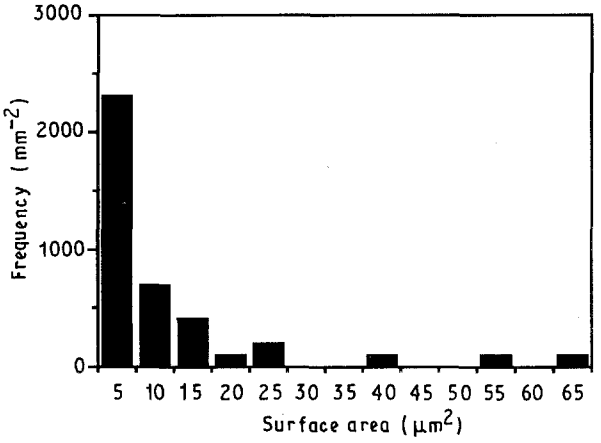

Figure 8 Histogram of pits surfaces on Sample C (molybdenum-ion implanted stainless steel after a 10 min immersion in 0.5 mol l^{-1} NaCl solution at the open potential then 180 s at 300 mV/SCE.)

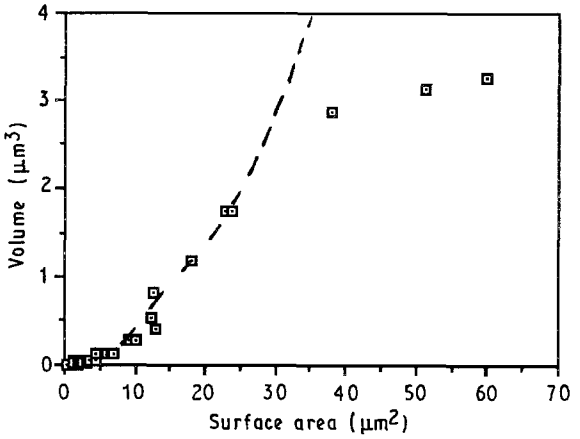

Figure 9 Surface–volume relation of pits on Sample C (molybdenum-ion implanted stainless steel after a 10 min immersion in 0.5 mol l^{-1} NaCl solution at the open potential then 180 s at 300 mV/SCE).

5. Conclusion

The corrosion of molybdenum-ion implanted and unimplanted stainless steel was studied by phase shifting interferometry microscopy (PSIM); on unimplanted material small dimension pits occur even at the corrosion potential; on implanted material both macroscopic pits and pre-pits exist if the potential is high (300–700 mV/SCE).

The PSIM is a well-adapted technique for the determination of geometrical characteristics of pits (surface, volume). Moreover, both statistical and evaluative studies are possible with this technique.

For unimplanted 304 stainless steel, the PSIM technique is complementary to other current electrochemical techniques. In fact for ion-implanted material, statistical standard electrochemical techniques cannot be used because they require a large number of samples. On the other hand, the optical techniques provide information about the whole surface of the sample. Consequently, it is possible to take into account each individual pit.

Optical methods assisted by microcomputers will probably be the subject of large developments in the future, particularly for ion-implanted materials.

Acknowledgements

This work was supported by the CNRS (GS Corrosion), UNIREC S.A. and UGINE-SAVOIE, which was greatly appreciated.

References

1. S. SKLARSKA-SMIALOWSKA, in "Pitting Corrosion of Metals", (National Association of Corrosion Engineers, 1986).

2. C. GABRIELLI, F. HUET, M. KEDDAM and R. OLTRA, *Corrosion* **46** (1990) 266.
3. P. FIEVET, Y. ROQUES and F. DABOSI, *C. R. Acad. Sci. Paris* **311** Série II (1990) 1327.
4. H. J. KRAGT, D. J. EARL, J. D. NORTON and H. S. WHITE, *J. Electrochem. Soc.* **136** (1989) 1752.
5. H. J. TIZIANI, *Opti. Quant. Electron.* **21** (1989) 253.
6. C. PIERALLI and G. TRIBILLON, *Signal Processing* **14** (1988) 69.
7. D. E. WILLIAMS, M. FLEISCHMANN, J. STEWART and T. BROOKS, in "Proceedings of International Symposium on Electrochemical Methods in Corrosion Research", July 1985, edited by G. E. Murch (Trans. Tech, Switzerland, 1986) p. 151.
8. C. GABRIELLI, F. HUET, M. KEDDAM, R. OLTRA and C. PALLOTTA, in "Passivity of Metals and Semiconductors", edited by M. Froment (Elsevier, Amsterdam, 1983) p. 293.
9. U. BERTOCCI and Y. X. YE, *J. Electrochem. Soc.* **131** (1984) 1011.

Received 1 August 1991
and accepted 7 April 1992